

Theoretical Study on Superconductivity in Boron-Doped Diamond

Tomonori SHIRAKAWA¹*, Satoshi HORIUCHI¹, Yukinori OHTA^{1,2} and Hidetoshi FUKUYAMA³

¹Graduate School of Science and Technology, Chiba University, Chiba 263-8522

²Department of Physics, Chiba University, Chiba 263-8522

³Department of Applied Physics, Tokyo University of Science, Kagurazaka, Tokyo 162-8601

We consider superconductivity in boron (B) doped diamond using a simplified model for the valence band of diamond. We treat the effects of substitutional disorder of B ions by the coherent potential approximation (CPA) and those of the attractive force between holes by the ladder approximation under the assumption of instantaneous interaction with the Debye cutoff. We thereby calculate the quasiparticle life time, the evolution of the single-particle spectra due to doping, and the effect of disorder on the superconducting critical temperature T_c . We in particular compare our results with those for supercell calculations to see the role of disorder, which turns out to be of crucial importance to T_c .

KEYWORDS: boron-doped diamond, superconductivity, disorder, coherent potential approximation

1. Introduction

Recent discovery of superconductivity in boron (B) doped diamond^{1,2)} has renewed interest in physics of doped semiconductors. Inelastic x-ray scattering experiment³⁾ indicates that the doped carriers are strongly coupled with bond-stretching phonons of $\omega \simeq 164$ meV associated with the covalent bonds into which the holes are doped. The relatively high critical temperature of $T_c \simeq 10\text{K}$ ^{4,5)} is remarkable in view of the expected small density of states at the Fermi energy ε_F due to small carrier density⁶⁾ as well as the existence of strong disorder intrinsic to the randomness in doped semiconductors.^{7,8)} In particular, the latter is deduced from the electrical resistivity measurement^{9–11)} and the line shape of quasi-particles observed by the angle-resolved photoemission spectroscopy (ARPES),¹²⁾ indicating that the life time of electrons τ is very short with the characteristic parameter of $\varepsilon_F\tau \lesssim 1$ (throughout this paper we set $\hbar = k_B = 1$) and violates the Ioffe-Regel criterion for coherent Bloch-like transport.^{7,8,11)} This small value of $\varepsilon_F\tau$ implies that the Fermi surface is not well-defined in momentum space but is blurred by scattering (see Fig. 1); the superconductivity in B-doped diamond may therefore be referred to as “superconductivity without Fermi surface”.¹³⁾

The strong scattering potential of the impurity B ions may be responsible not only for such disorder-induced anomalous features but also for the basic electronic states. The energy level of a single B impurity in diamond is very deep, locating at 0.37 eV above the top of the valence band of diamond,^{14,15)} and, in the presence of such a strong scattering potential, the simple picture of the ‘rigid-band shift’ of the Fermi level due to doping (or the virtual crystal approximation) based on the first-principles LDA (local-density approximation) band calculations^{16–18)} with the adjusted chemical potential may not necessarily be justified. In fact, some spectroscopic experimental data^{19–21)} seem to suggest the presence of non-rigid-band-like features reminiscent of the impurity states even in the metallic regime of B-doped diamond,

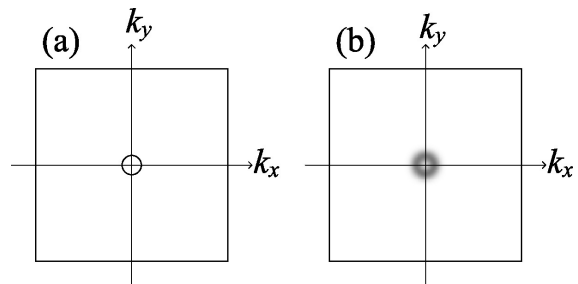


Fig. 1. Schematic representation of the Fermi surface in the two-dimensional analogue of the Brillouin zone for hole-doped diamond; (a) without disorder, a small Fermi surface is present, but (b) with disorder, the Fermi surface is smeared out by scattering.

which has been focused upon by Baskaran.^{7,8)} Hence, evolution of the impurity states due to doping should be accessed with more care.

Another key feature is the observed very small carrier concentration. A recent analysis of the NMR spectra⁶⁾ suggests that the real doping rate of carriers (or the number of carriers per site) is at most only $\sim 1\%$, which differs very much from the nominal doping rates of $\sim 5\%$, and that this is due to the formation of boron-hydrogen (BH) complex; i.e., H atoms inevitably introduced in the synthetic processes of the materials absorb the holes introduced by B impurities. This possibility has been suggested recently both theoretically and experimentally; an LDA calculation has shown that the B ions occupy the carbon sites substitutionally and the H ions sit on the interstitial positions between B ions and the neighboring carbon ions,²²⁾ and based on the assumption of the presence of these two types of B ions, the observed NMR spectra can be analyzed consistently.⁶⁾ We should therefore reexamine the electronic states of B-doped diamond, in particular, in the regime of low carrier concentration of $\sim 1\%$, starting from the dilute limit of B doping.

In this paper, we will first study the electronic states of this highly disordered system, based on a simplified model for the valence band of diamond by use of the co-

*E-mail address: sirakawa@physics.s.chiba-u.ac.jp

herent potential approximation (CPA) for treating the effects of the substitutional disorder of B ions. We thereby calculate the density of states, life time, and evolution of the single-particle spectra due to doping, the results of which are compared with available experimental data including ARPES spectra.

We will also calculate the superconducting pairing susceptibility based on the ladder approximation under the assumption of instantaneous interaction and estimate the doping dependence of the critical temperature T_c . We thereby want to clarify the effects of disorder on the superconductivity in such unusual situations as described above. We will in particular compare our results with those for supercell calculations (i.e., the periodic arrangement of B ions) to see the role of disorder, which turns out to be of crucial importance. Here we do not pursue processes of the attractive interaction in detail, though we assume it is due to the electron-phonon interaction associated with bond-stretching modes with very high frequency, as has been indicated both experimentally and theoretically.^{3, 16–18, 23)} Preliminary results of our work have been presented in ref.²⁴⁾

This paper is organized as follows. In §2, we present our model and method of calculations. In particular, we derive the pairing susceptibility within the framework of CPA. In §3, we present our results of calculations for the density of states, life time, single-particle spectra, and superconducting critical temperature, which are compared with available experimental data in §4. Discussions are given in §5, and we summarize our work in §6.

2. Method of Calculations

2.1 Model

In order to extract the effects of disorder on the electronic states near the top of the valence bands of diamond, we assume, for the sake of simplicity, the tight-binding model based on the simple cubic structure. By this simplification, the degeneracy of three bands at the top of the valence bands of diamond is ignored. However, we believe that the essential features of the effects of disorder can be taken into account in this simple model.

Adding the random potential Δ at B sites and the on-site attractive interaction $-V$ ($V > 0$), our model may be written by the Hamiltonian

$$\mathcal{H} = \sum_{\mathbf{k}\sigma} (\varepsilon_{\mathbf{k}} - \mu) c_{\mathbf{k}\sigma}^\dagger c_{\mathbf{k}\sigma} + \Delta \sum_{i \in B} \sum_{\sigma} n_{i\sigma} - V \sum_i n_{i\uparrow} n_{i\downarrow} \quad (1)$$

with

$$\varepsilon_{\mathbf{k}} = t (\cos k_x a + \cos k_y a + \cos k_z a), \quad (2)$$

where $n_{i\sigma}$ is the number operator at site i and spin σ and $c_{\mathbf{k}\sigma}^\dagger$ creates an electron with momentum \mathbf{k} and spin σ , μ is the chemical potential.

Hereafter, we assume $t = 1$ as the unit of energy unless otherwise indicated; to reproduce the width of the valence band of diamond 22 eV, this choice corresponds to taking 3.7 eV as the unit of energy. The effective mass at the top of the valence band of diamond is roughly reproduced by this choice.

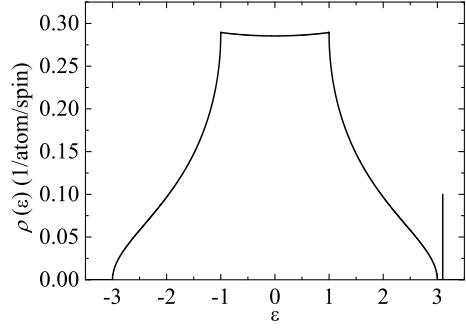


Fig. 2. Model density of states for the tight-binding band on the three-dimensional simple cubic lattice without disorder. Energy level of a single impurity is also shown.

We determine the value of Δ so as to reproduce the energy level of B ions in the dilute limit, which is experimentally known to be located at 0.37 eV above the top of the valence band of pure diamond;^{14, 15)} we obtain the value $\Delta = 2.30$, which is used throughout the present work. The density of states of this model is shown in Fig. 2 with the energy level of a single B impurity. The sites with Δ are distributed randomly over the lattice sites of the simple cubic structure; this substitutional disorder is treated by CPA. We define the concentration of B ions as $c_B = N_B/N$ where N_B is the number of B sites and N is the total number of sites in the system.

2.2 Coherent Potential Approximation

Let us assume the absence of the attractive interaction, i.e., $V = 0$, for the moment. In CPA, the Green's function is defined with the momentum-independent self-energy function $\Sigma(i\varepsilon_n)$ as

$$G^{-1}(\mathbf{k}, i\varepsilon_n) = i\varepsilon_n - \varepsilon_{\mathbf{k}} + \mu - \Sigma(i\varepsilon_n) \quad (3)$$

where $\varepsilon_{\mathbf{k}}$ is the band structure without impurities eq. (2), μ is chemical potential, and $\varepsilon_n = (2n + 1)\pi/\beta$, with $\beta = 1/T$. The self-energy function in the presence of the substitutional disorder is given as the polynomial series expansion^{25–27)} as shown in Fig. 3(a):

$$\Sigma(i\varepsilon_n) = \Delta \sum_{S=1}^{\infty} Q_S(c_B) \Delta^{S-1} \Theta^{S-1}(i\varepsilon_n) \quad (4a)$$

$$= \frac{c_B \Delta}{1 - \Theta(i\varepsilon_n)(\Delta - \Sigma(i\varepsilon_n))} \quad (4b)$$

where

$$\Theta(i\varepsilon_n) = \frac{1}{N} \sum_{\mathbf{k}} G(\mathbf{k}, i\varepsilon_n) \quad (5)$$

and $Q_S(c_B)$ is the polynomial of c_B . In the following, we use abbreviations $\Sigma = \Sigma(i\varepsilon_n)$ and $\Theta = \Theta(i\varepsilon_n)$.

The CPA equation for Σ

$$\Theta \Sigma^2 + (1 - \Delta \Theta) \Sigma - c_B \Delta = 0. \quad (6)$$

is solved numerically by use of eq. (2).

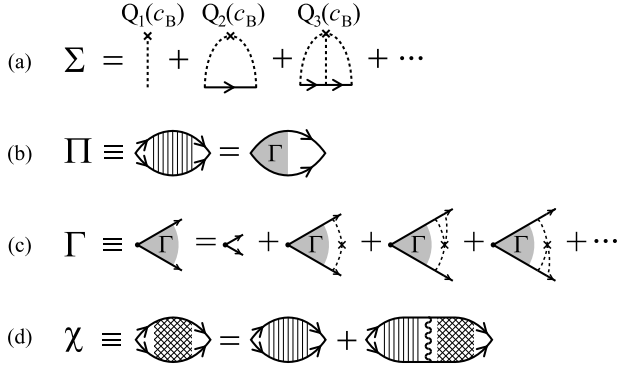


Fig. 3. (a) The self-energy Σ by CPA. Dotted and solid lines represent the perturbation potential Δ and Green's function, respectively, and \times represents $Q_S(c_B)$. (b) Diagram for the pairing susceptibility Π given in eq. (8). (c) Diagram for determining the vertex function Γ in eq. (10). (d) Diagram for the pairing susceptibility χ by the ladder approximation eq. (18). Wavy line represents the attractive interaction V .

2.3 Pairing Susceptibility by CPA

We consider the pairing (or Cooper-pair) susceptibility in the absence of V defined as

$$\Pi(\mathbf{q}, i\omega_m) = \int_0^\beta d\tau e^{i\omega_m\tau} \langle T_\tau b_{\mathbf{q}}^\dagger(\tau) b_{\mathbf{q}} \rangle \quad (7)$$

with $b_{\mathbf{q}} = \sum_{\mathbf{k}} c_{-\mathbf{k}-\mathbf{q}/2, \downarrow} c_{\mathbf{k}-\mathbf{q}/2, \uparrow}$ and $\omega_m = 2\pi m/\beta$. Following the CPA theory for the magnetic susceptibility,^{28,29} we find that eq. (7) is given by

$$\Pi(\mathbf{q}, i\omega_m) = T \sum_n \sum_{\mathbf{k}} G G_+ \Gamma \quad (8)$$

with

$$G = G(\mathbf{k}, i\varepsilon_n) \quad (9a)$$

$$G_+ = G(-\mathbf{k} + \mathbf{q}, -i\varepsilon_n + i\omega_m) \quad (9b)$$

$$\Gamma = \Gamma(\mathbf{q}, i\varepsilon_n, i\omega_m), \quad (9c)$$

which is illustrated in Fig. 3(b). The vertex function Γ is determined by the equation (see Fig. 3(c)):

$$\Gamma = 1 + \Gamma A \\ \times \sum_{S=2}^{\infty} \Delta^S Q_S (\Theta^{S-2} + \Theta^{S-3} \Theta_+ + \dots + \Theta_+^{S-2}) \quad (10)$$

with

$$\Theta_+ = \Theta(-i\varepsilon_n + i\omega_m) \quad (11a)$$

$$A = A(\mathbf{q}, i\varepsilon_n, i\omega_m) = \frac{1}{N} \sum_{\mathbf{k}} G G_+. \quad (11b)$$

Equation (10) is solved for Γ as

$$\Gamma = \left(1 - A \frac{\Sigma - \Sigma_+}{\Theta - \Theta_+} \right)^{-1} \quad (12)$$

with

$$\Sigma_+ = \Sigma(-i\varepsilon_n + i\omega_m). \quad (13)$$

We thus obtain

$$\Pi(\mathbf{q}, i\omega_m) = T \sum_n A(\mathbf{q}, i\varepsilon_n, i\omega_m) \Gamma(\mathbf{q}, i\varepsilon_n, i\omega_m) \quad (14)$$

for the pairing susceptibility in the absence of attractive interactions. Since we have

$$A(0, i\varepsilon_n, 0) = \frac{\Theta(-i\varepsilon_n) - \Theta(i\varepsilon_n)}{2i\varepsilon_n + \Sigma(-i\varepsilon_n) - \Sigma(i\varepsilon_n)} \quad (15a)$$

$$\Gamma(0, i\varepsilon_n, 0) = \frac{2i\varepsilon_n + \Sigma(-i\varepsilon_n) - \Sigma(i\varepsilon_n)}{2i\varepsilon_n} \quad (15b)$$

from eqs. (11) and (12), we see from eq. (14) that the pairing susceptibility for $\mathbf{q} = 0$ and $i\omega_m = 0$ is given as follows;

$$\Pi(0, 0) = T \sum_n \frac{\Theta(-i\varepsilon_n) - \Theta(i\varepsilon_n)}{2i\varepsilon_n} \quad (16a)$$

$$= \frac{1}{2} \int d\varepsilon \rho(\varepsilon) \frac{1}{\varepsilon - \mu} \tanh\left(\frac{\beta(\varepsilon - \mu)}{2}\right) \quad (16b)$$

where

$$\rho(\varepsilon) = -\frac{1}{\pi} \lim_{\delta \rightarrow 0^+} \text{Im} \frac{1}{N} \sum_{\mathbf{k}} G(\mathbf{k}, \varepsilon - \mu + i\delta). \quad (17)$$

We thus find that the effects of disorder in the present approximation appear only through the density of states in disordered systems, $\rho(\varepsilon)$.

We should note that the vertex correction Γ is essential here; if we take into account the effects of disorder only from the self-energy via A , the value of the pairing susceptibility $\Pi(0, 0)$ becomes very small (reflecting the effects of disorder too strongly), but the vertex correction, which becomes very large around the Fermi energy, recovers the value of $\Pi(0, 0)$, to result in the BCS form of the pairing susceptibility eq. (16). Thus, the effects of disorder, even though it is strong, can be renormalized solely into the density of states $\rho(\varepsilon)$. This cancellation is just as in the case of the calculation of the magnetic susceptibility.^{28,29}

In the presence of the attractive interaction, $V > 0$, the pairing susceptibility at $\mathbf{q} = 0$ and $i\omega_m = 0$, $\chi(T)$, is given in the ladder approximation by the process shown in Fig. 3(d), which results in

$$\chi(T) = \frac{\Pi(0, 0)}{1 - V\Pi(0, 0)}. \quad (18)$$

The critical temperature T_c is determined from the condition $V\Pi(0, 0) = 1$ at which $\chi(T)$ diverges: i.e.,

$$\frac{1}{V} = \frac{1}{2} \int d\varepsilon \rho(\varepsilon) \frac{1}{\varepsilon - \mu} \tanh\left(\frac{\beta(\varepsilon - \mu)}{2}\right). \quad (19)$$

Note that our result for $\Pi(0, 0)$ can be considered as an extension of Anderson's theorem³⁰ which states that T_c of an isotropic s -wave superconductor is not affected by nonmagnetic impurities if the density of states is unchanged by scattering. The extension is that, within CPA, even the strong disorder that deforms the density of states does not affect the validity of the BCS expression eq. (16) for the pairing susceptibility.

3. Results of Calculations

3.1 Density of States and Self-energy

Calculated results for the density of states are shown in Fig. 4. We find that the impurity states broaden and get weight continuously as the doping rate is increased.

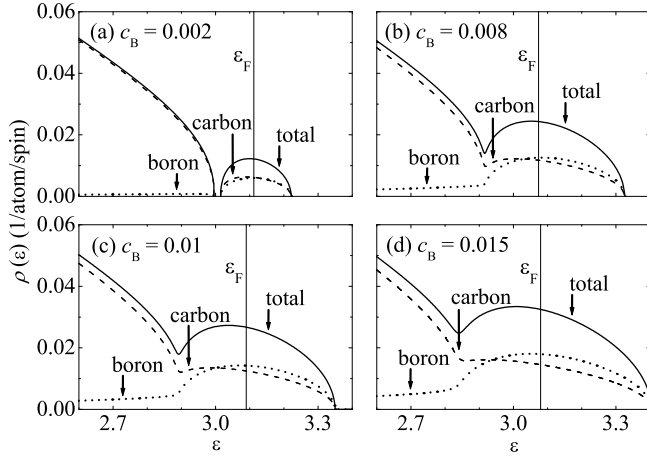


Fig. 4. Density of states $\rho(\varepsilon)$ near the Fermi energy calculated by CPA. Local densities of states for carbon and boron sites are also shown. The vertical line indicates the Fermi energy ε_F in the absence of compensation.

The broadening is due to the large imaginary part of the self-energy around the Fermi energy (see below). The impurity states are separated from the top of the valence band up to the doping rate of $c_B \simeq 0.2\%$ (see Fig. 4(a)), but are merged into the top of the valence band with increasing doping. The weight of the impurity states corresponds to the doping concentration. We assume the absence of compensation hereafter; i.e., the doping rate of holes is equal to c_B . Then, the Fermi energy ε_F at $T = 0$ K (then $\mu = \varepsilon_F$) is determined by

$$\int_{-\infty}^{\varepsilon_F} \rho(\varepsilon) d\varepsilon = 1 - \frac{c_B}{2}. \quad (20)$$

Thus, the impurity states, if they are detached from the valence bands, are at half filling, as pointed out in ref..⁷⁾

$$\frac{1}{c_B \Delta} \left[\text{Diagram 1} + \text{Diagram 2} + \text{Diagram 3} + \dots \right]$$

Fig. 5. (a) Diagram for defining the local density of states at B site, $\rho_B(\varepsilon)$. Dotted and solid lines represent the perturbation potential Δ and Green's function, respectively, and \times represents $Q_S(c_B)$.

The local density of states for B sites may be defined as in Fig. 5 and is given by

$$\rho_B(\varepsilon) = -\frac{c_B}{\pi} \text{Im} \frac{1}{c_B \Delta} \sum_{S=1}^{\infty} Q_S(c_B) \Delta^S \Theta^S(\varepsilon - \mu + i\delta) \quad (21a)$$

$$= -\frac{c_B}{\pi} \text{Im} \frac{\Theta(\varepsilon - \mu + i\delta)}{1 - (\Delta - \Sigma(\varepsilon - \mu + i\delta)) \Theta(\varepsilon - \mu + i\delta)} \quad (21b)$$

with $\delta \rightarrow 0^+$. The local density of states for carbon sites may be defined as $\rho_C(\varepsilon) = \rho(\varepsilon) - \rho_B(\varepsilon)$. The calculated results are shown also in Fig. 4, where we find that the boron component is concentrated on the impurity states

but the carbon component in the states is as large as the boron component.

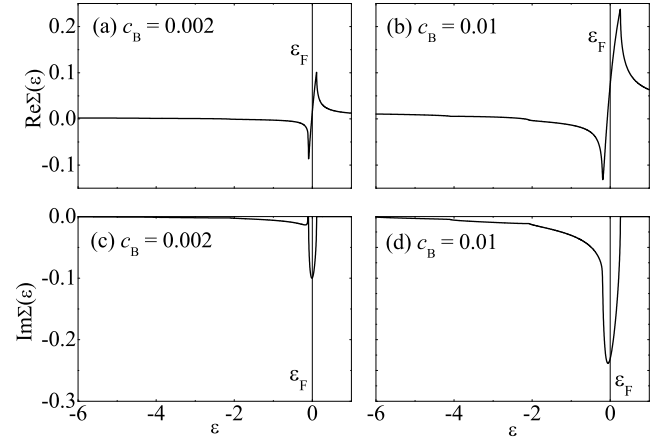


Fig. 6. Calculated real (upper panels) and imaginary (lower panels) parts of the self-energy $\Sigma(\varepsilon)$ by CPA. The vertical line indicates the Fermi energy in the absence of compensation.

The real and imaginary parts of the self-energy $\Sigma(\varepsilon)$ are shown in Fig. 6, where we find that there is a large imaginary part $-\text{Im}\Sigma(\varepsilon)$ in the impurity states, which are responsible for the broadening of the density of states of the impurity states, as well as for the short life time of electrons (see below).

3.2 Life Time and Mean-Free-Path

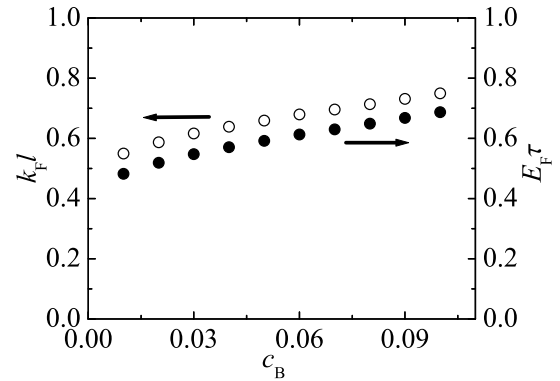


Fig. 7. Calculated life time $E_F \tau$ (●) and mean-free-path $k_F \ell$ (○) as a function of c_B .

The life time τ at the Fermi energy ε_F may be defined as

$$\tau = -\frac{1}{2 \text{Im} \Sigma(\varepsilon_F + i\delta)} \quad (22)$$

with $\delta \rightarrow 0^+$, the value of which is determined directly from the imaginary part of the self-energy calculated at ε_F in the presence of disorder. By use of this τ , the mean-free-path $\ell = v_F \tau$, $E_F \tau$, and $k_F \ell$ may be defined with v_F , k_F , and E_F being the Fermi velocity, Fermi wavevector, and Fermi energy, respectively, corresponding to the same carrier number but in the absence of disorder.

The calculated results for $E_F\tau$ and $k_F\ell$ are shown in Fig. 7 as a function of c_B , where we find that τ and ℓ are indeed very short, irrespective of the doping rates, which comes from the large imaginary part of the self-energy at the Fermi energy (see Fig. 6). At $c_B = 0.01$, e.g., we have the values $E_F\tau \simeq 0.48$ and $k_F\ell \simeq 0.55$.

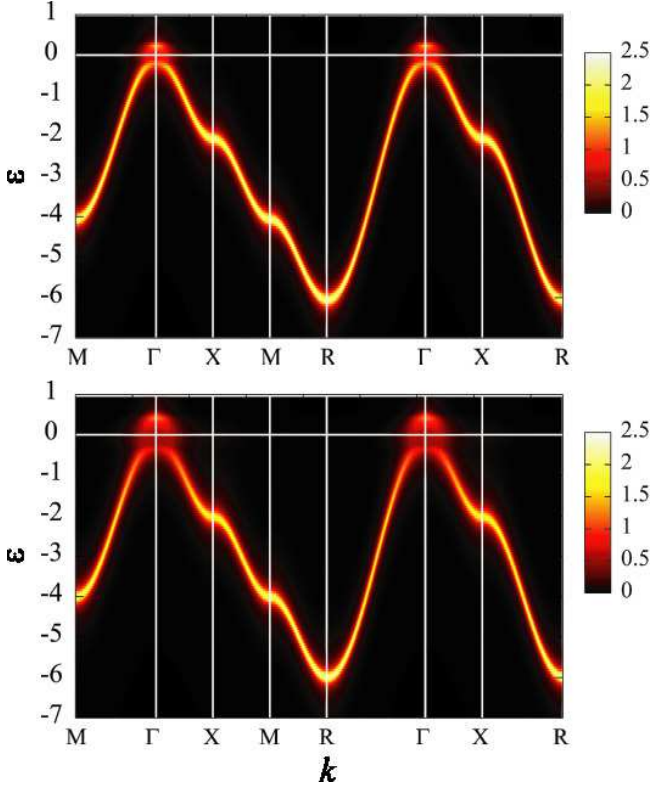


Fig. 8. (Color online) Calculated results for the single-particle spectra $\rho(\mathbf{k}, \varepsilon)$ at $c_B = 0.01$ (upper panel) and $c_B = 0.03$ (lower panel). The artificial broadening of $\delta = 0.13$ is included in the spectra for the illustrative purpose.

3.3 Single-Particle Spectra

The calculated single-particle spectra are shown in Fig. 8, where we illustrate the quantity

$$\rho(\mathbf{k}, \varepsilon) = -\frac{1}{\pi} \text{Im} G(\mathbf{k}, \varepsilon + i\delta), \quad (23)$$

by which we can envisage the broadening of the band structure due to disorder in the Brillouin zone as well as the location of spectral weight due to the impurity states. We find that the impurity states are clearly seen just above the top of the valence band. We note that the impurity states are fairly localized in momentum space around the Γ point even at very low doping rates. This result will be compared later with the results of the ARPES experiment.¹²⁾

3.4 Superconducting Critical Temperature

The superconducting critical temperature T_c is calculated from eq. (19) together with the chemical potential μ determined from

$$\int_{-\infty}^{\infty} d\varepsilon f(\varepsilon)\rho(\varepsilon) = 1 - \frac{c_B}{2} \quad (24)$$

with $f(\varepsilon) = 1/(e^{\beta(\varepsilon-\mu)} + 1)$. Here, we assume the Debye cutoff of $\omega_D = 2300$ K corresponding to the bond-stretching mode; i.e., the energy integral of eq. (16) is from $\varepsilon = \mu - \omega_D$ to $\mu + \omega_D$. The calculated results for T_c are shown in Fig. 9 as a function of c_B for various values of the attractive interaction V . We find that the value of T_c increases rapidly with doping rate c_B and the attractive interaction V . If the energy of the bond-stretching mode of diamond $\omega = 164$ meV is used as the cutoff energy in the integral of eq. (16), the value of T_c is found to decrease by $\sim 30\%$ but the general trend seen in Fig. 9 does not change.

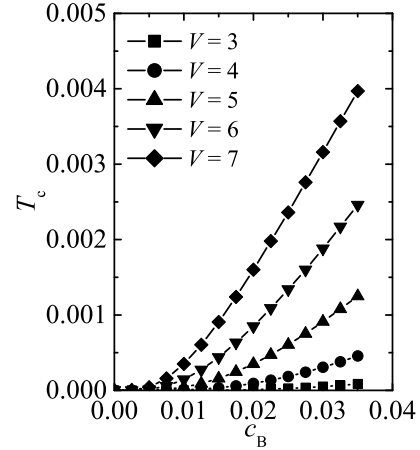


Fig. 9. Superconducting critical temperature T_c as a function of c_B calculated by CPA.

Our results may be compared with results of the first-principles LDA calculations based on either virtual crystal approximation^{16,17)} or supercell method.^{17,18)} We find that our value of the density of states at the Fermi energy $\rho(\varepsilon_F)$ is about a factor 5 smaller than the values of the LDA calculations¹⁶⁾ if we compare at doping rate of $c_B = 0.03$. The causes of this difference are the following; the absence of the three-fold degeneracy on one hand and the effects of disorder on the other hand in the present calculations. Actually, for the latter, we have the value $\rho(\varepsilon_F) = 0.027$ (0.046) at, e.g., $c_B = 0.01$ (0.03) in our CPA calculation, while without disorder in the same model, we have $\rho(\varepsilon_F) = 0.035$ (0.053) at $c_B = 0.01$ (0.03).

The strength of the electron-phonon coupling constant λ has also been estimated by the LDA calculations,¹⁶⁻¹⁸⁾ where it was found that the contribution stems predominantly from the bond-stretching phonon mode and that the values are $\lambda \simeq 0.3 - 0.55$ at $c_B \simeq 0.02 - 0.03$. The value of T_c has thereby been estimated based on the BCS or McMillan's formula³²⁾ and found to be in quantitative agreement with experiment.¹⁶⁻¹⁸⁾ Then, from the comparison with the results of the LDA calculations, the strength of the attractive interaction V in our theory may be estimated; i.e., by using the relation³²⁾

$$\rho(\varepsilon_F)V = \frac{\lambda - \mu^*}{1 + \lambda} \quad (25)$$

with our calculated value of $\rho(\varepsilon_F) = 0.027$ at $c_B = 0.01$ and a standard value of the Coulomb pseudopotential parameter $\mu^* \simeq 0.1$, and by assuming a typical value of the electron-phonon coupling constant $\lambda \simeq 0.31$ at $c_B = 0.01$, we can estimate the value of the attractive interaction to be $V \simeq 6$.

4. Comparisons with Experiment

4.1 Density of States

The calculated results for the density of states (see Fig. 4) may be compared with results of a number of spectroscopy experiments such as the photoemission and absorption spectra^{12, 19, 20, 31}) and optical conductivity spectra.²¹) Although the effects of the matrix elements relevant to each experiment is not taken into account in the present calculations, the comparison can offer important information on the impurity states of the hole-doped diamond.

We first point out that our calculated results for the density of states (see Fig. 4) indicate that the impurity states evolve continuously by doping from the low-doping limit, where it has been established^{14, 15}) that the triply-degenerate impurity level exists for a single B impurity in otherwise pure diamond. This is in contrast to the claim of the rigid-band shift of the Fermi energy suggested in the first-principles LDA band calculations by the supercell method,^{17, 18}) which cannot reproduce the separated impurity level at low doping limit of diamond.²²)

The presence or absence of the impurity states in the metallic regime of B-doped diamond should in principle be clarified by experiment. First, the angle-integrated photoemission spectroscopy experiment³¹) has not so far provided evidences for the presence of the impurity states. On the other hand, the X-ray absorption (XAS) and emission (XES) spectroscopy experiments^{19, 20}) seem to suggest the presence of the impurity states⁸) although not yet fully conclusive. The optical conductivity experiment²¹) also seems to support the presence of the impurity states even in the metallic regime, where it has been found that, by doping, there appear the broad spectral features at ~ 0.37 eV that may correspond to the impurity states while the Drude weight is hardly visible.

Further experimental studies are desired to clarify the nature of the impurity states in B-doped diamond.

4.2 Life Time and Mean-Free-Path

The calculated results for the life time and mean-free-path are shown in Fig. 7. At $c_B = 0.01$, e.g., we find the values $E_F\tau = 0.48$ and $k_F\ell = 0.55$. These values of $E_F\tau$ and $k_F\ell$ are close to the experimental values $E_F\tau = 0.27$ and $k_F\ell = 0.32, 0.48$, and 1.0 for the three bands obtained from the line shape of quasiparticles by ARPES experiment for the highest T_c sample.¹²) The analyses of the measured resistivity^{2, 9-11}) lead to similar small values of $E_F\tau$ and $k_F\ell$ as well.

4.3 Angle-Resolved Photoemission Spectra

The calculated results for the single-particle spectra in Fig. 8 may be compared with the experimental ARPES spectra given in Fig. 2 of ref.¹²) To do this, we recalculate the spectra by convoluting calculated results with

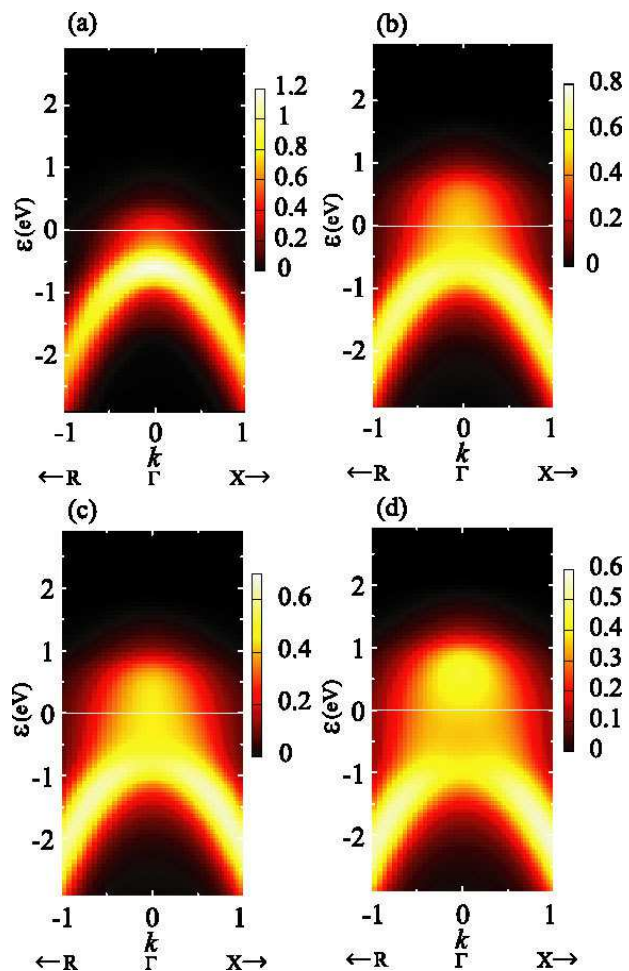


Fig. 10. (Color online) Calculated results for the single-particle spectra $\rho(\mathbf{k}, \varepsilon)$ at doping rates of (a) $c_B = 0.2\%$, (b) $c_B = 0.8\%$, (c) $c_B = 1.0\%$, and (d) $c_B = 1.5\%$. The finite resolutions in both energy (250meV) and momentum ($\pm 0.026\text{au}^{-1}$) in experiment¹²) are taken into account in the calculation. The spectra below the Fermi energy (shown by horizontal line) may be compared with the experimental ARPES data obtained by Yokoya *et al.*¹²) The unit of energy is given in eV for comparison with experiment. Horizontal axes are in units of $1/a$.

the experimental resolutions in both energy (250 meV) and momentum ($\pm 0,026 \text{ au}^{-1}$) in view of the actual experiment.¹²) The results near the Fermi energy are shown in Fig. 10, where the spectra both below (which can be compared with experiment) and above the Fermi energy are presented. We should stress again that the three-fold degeneracy of the top of the valence band is ignored in our calculations. We find however that the agreement between theory and experiment (below the Fermi energy) is obviously reasonable; i.e., even in the presence of the impurity states, the spectra of the valence band indeed look just as if the rigid-band shift of the Fermi energy were operating. But this apparent agreement does not imply that the impurity states are not present. This is in particular the case at low-doping regions; at $c_B = 0.2\%$, the impurity states are not clearly identified in the calculated angle-resolved spectra (see Fig. 10(a)), but in the calculated density of states (see Fig. 4(a)), we find that the impurity states certainly exist, which are separated from the top of the valence band. Thus, up to the dop-

ing rates of $c_B \simeq 1\%$, the shape of the angle-resolved spectra below the Fermi energy is not largely modified by the presence of the impurity states. We therefore consider that the claim¹²⁾ of the absence of the impurity states made from their ARPES data may not be justified, at least with resolutions in both momentum and energy used in the actual experiments. Further experiments with much higher resolutions would be able to resolve the issue.

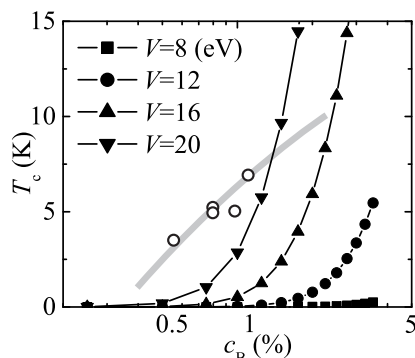


Fig. 11. Comparison between the calculated critical temperature T_c as a function of c_B and the experimental data (open circles and broad curve) estimated by Mukuda *et al.*⁶⁾ from the analysis of the NMR spectra. T_c is given in units of K for comparison with experiment. The values of V used for calculations are given in units of eV here.

4.4 Superconducting Critical Temperature

The calculated results for the doping dependence of T_c are compared with experiment in Fig. 11. We find that if we assume an appropriate value of V , e.g., $V \simeq 6$ (which corresponds to ~ 20 eV), our result of $T_c \simeq 7$ K at $c_B = 1\%$ is in reasonable agreement with results of the LDA calculations^{16–18)} and therefore with experiment. In particular, we find that the rapid increase in T_c with increasing doping rate, which is observed in experiment, is reproduced fairly well.

If seen more quantitatively, however, one may notice that the calculated concave dependence of T_c on c_B (see Fig. 11) is somehow not consistent with experiments where the nearly linear dependence on c_B in the logarithmic scale is seen. We consider that the discrepancy may partly be due to the insufficiency (or mean-field nature) of CPA. In CPA, both the width and height of the density of states of the impurity states vary as $\sim \sqrt{c_B}$ (hence, the area varies as $\sim c_B$), whereas in reality, there is a tendency^{33–35)} that the width varies as $\sim c_B$ and the height is almost kept constant ~ 1 . If we take into account this tendency in our calculations, the agreement between theory and experiment will be improved.

5. Discussions

In this section, we want to discuss some issues and possibilities.

First, let us consider possible improvements of our calculations presented in this paper. We should first of all point out that our calculated values of T_c are not of

sufficient quantitative significance since the calculations are based on the single-band model of the simple-cubic lattice and the instantaneous interaction for the attractive force. For more quantitative estimation of T_c , we may need the following improvements: (i) The nearly-degenerate three-band structure around the top of the valence band of diamond in the actual lattice structure should be included. (ii) The retardation effects for the electron-phonon coupling should be taken into account. (iii) The dynamical aspect of the Coulomb interaction between holes should be important; due to the effects of diffusion by randomness, the Coulomb pseudopotential parameter μ^* should be effectively larger.^{36,37)} (iv) Approximations beyond CPA will be desirable as pointed out in §4.4. These subjects deserve further studies.

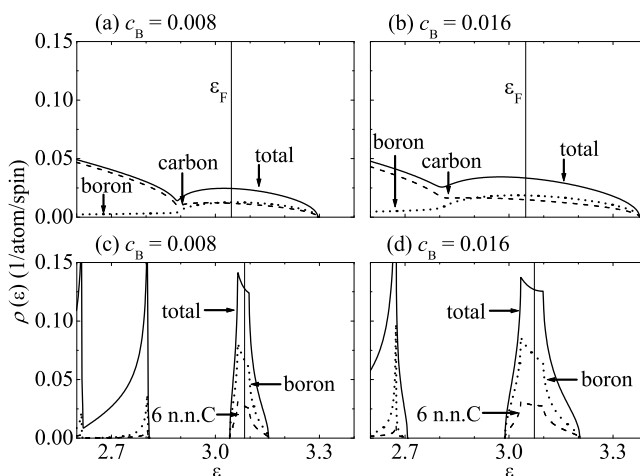


Fig. 12. Densities of states near the Fermi energy obtained by CPA (upper panels) and those calculated under the assumption of the periodic arrangement of B ions (lower panels). The $5 \times 5 \times 5$ and $4 \times 4 \times 4$ supercells are assumed in (c) and (d), respectively. Partial densities of states are also shown where ‘6 n.n.C’ means the partial density of states summed over the six nearest-neighbor carbon sites around a boron ion. Vertical lines indicate the Fermi energy ϵ_F .

Next, let us consider what happens to T_c if there were no effects of disorder of B ions. To see this, we carry out the supercell calculations for the same set of parameter values used in the CPA calculations. The B ions are arranged periodically by using $6 \times 6 \times 6$, $5 \times 5 \times 5$, $4 \times 4 \times 4$, and $3 \times 3 \times 3$ supercells of the simple-cubic lattice, which correspond to 0.46%, 0.80%, 1.56%, and 3.7% doping rates, respectively. The calculated results for the density of states are shown in Fig. 12, which are compared with the results of CPA at the same doping rates. We find that a rather narrow density of states for the impurity states appears above the top of the valence band, which form bands (impurity band), and that the density of states at the Fermi energy is much higher than the result of the CPA calculation. The separation between the impurity band and the top of the valence band is ~ 1 eV, which is significantly larger than the energy of the impurity level in the dilute limit, 0.37 eV, due to level repulsions.

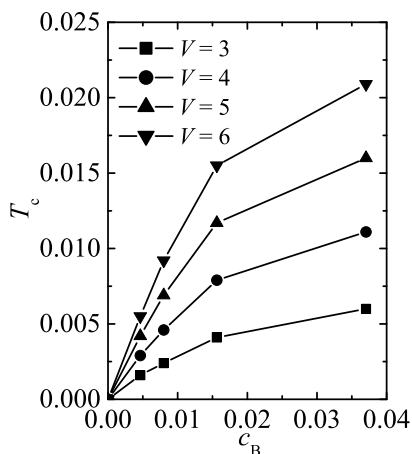


Fig. 13. Superconducting critical temperature T_c obtained under the assumption of the periodic arrangement of B ions.

We then calculate the values of T_c for these supercell systems by using eq. (19). The results are shown in Fig. 13. We find that the obtained values of T_c are nearly an order of magnitude higher than the results of the CPA calculations for the same attractive strength (see Fig. 9). Thus, we may conclude that, if impurity B ions could be arranged periodically, one would be able to have the critical temperature of an order of ~ 100 K. This value of T_c exceeds $T_c \simeq 30 - 40$ K of what is called the theoretical limit of the BCS theory for conventional superconductors; this is not surprising because the Debye frequency of diamond $\omega_D = 2300$ K is exceptionally large, together with the presence of the strong electron-phonon coupling because of the hole doping into the covalent bonds.¹³⁾ In other words, we can say that, in actual B-doped diamond, the effect of disorder indeed strongly suppresses the value of T_c . Note the ‘convex’ dependence of T_c on c_B in Fig. 13, which is in contrast to that of the CPA calculation where the dependence is ‘concave’ (see Fig. 9); i.e., the T_c in the supercell calculations decreases very rapidly with decreasing c_B . This comes from the narrow density of states of the impurity band, where the width of the impurity band becomes less than the Debye cutoff and the integral in eq. (19) becomes very small.

Together with reduction of the effects of disorder to raise T_c , the increase of hole concentration is obviously another way. In the actual experiment, one may try to find out way to remove or reduce the H atoms introduced in the synthetic processes of the materials; i.e., the reduction of passivation rate.

Finally, we want to point out the possibility of the occurrence of superconductivity in similar covalent-bonded materials. Based on the present study, we may suggest that the doping of carriers in boron-nitride (BN) and silicon-carbide (SiC) may be quite interesting; these materials with the cubic (zinc-blende) structure not only have the valence-band structure with a large band gap similar to diamond but also have the bond-stretching phonon mode with very high frequency.^{38–44)} Then, we may expect that the doping of enough carriers would lead to superconductivity with appreciable T_c .

6. Conclusions

We have studied the superconductivity in B-doped diamond by use of CPA for treating the substitutional disorder of B ions and by treating the attractive force between holes by the ladder approximation under the assumption of instantaneous interaction. The main messages obtained from our studies are the following:

(i) The effects of disorder are essential for understanding the electronic state of B-doped diamond. The broadening of the density of states and single-particle spectra near the Fermi energy, as well as the very short life-time and mean-free-path, are due to the effects of disorder, i.e., the large imaginary part of the self-energy induced by the disorder of B ions.

(ii) The pairing susceptibility derived by CPA takes the form of the BCS theory, where the effects of disorder are renormalized solely into the density of states, even in the presence of strong disorder that deforms the shape of the density of states. The vertex correction is found to be essential here: i.e., the susceptibility becomes too small if we take into account only the effect of the self-energy, but it is recovered by the vertex correction, leading to the BCS expression for the pairing susceptibility.

(iii) The superconducting critical temperature T_c can be raised substantially by reducing the effects of disorder in doping processes, e.g., by controlled spatial arrangement of B ions.

We believe that the doped semiconductors should have capabilities for producing a new class of superconducting materials and therefore we hope that our work presented here will encourage further experimental studies of superconductivity induced by doping into covalent-bonded semiconductors.

Acknowledgment

One of the authors (H.F.) thanks G. Baskaran for initial input and various discussions and M. Dresselhaus for informative discussion regarding C-related materials. Discussions on experimental facts with S. Shin in early stage are also acknowledged. Thanks are also due to E. Bustarret, K. Ishizaka, K. Miyake, J. Mizuki, H. Mukuda, J. Nakamura, T. Oguchi, Y. Takada, Y. Takano, N. Yamada, and T. Yokoya. T. S. acknowledges support from Mochizuki Foundation. This work was supported in part by Grants-in-Aid for Scientific Research (Nos. 16076201 and 18540338) from the Ministry of Education, Science, Sports, and Culture of Japan. A part of computations was carried out at the Research Center for Computational Science, Okazaki Research Facilities, and the Institute for Solid State Physics, University of Tokyo.

- 1) E. A. Ekimov, V. A. Sidorov, E. D. Bauer, N. N. Mel’nik, N. J. Curro, J. D. Thompson, and S. M. Stishov: *Nature (London)* **428** (2004) 542.
- 2) Y. Takano, M. Nagao, I. Sakaguchi, M. Tachiki, T. Hatano, K. Kobayashi, H. Umezawa, and H. Kawarada: *Appl. Phys. Lett.* **85** (2004) 2851.
- 3) M. Hoesch, T. Fukuda, T. Takenouchi, J. P. Sutter, S. Tsutsui, A. Q. R. Baron, M. Nagao, Y. Takano, H. Kawarada, and J. Mizuki: *cond-mat/0512424*.

- 4) Y. Takano, M. Nagao, T. Takenouchi, H. Umezawa, I. Sakaguchi, M. Tachiki, and H. Kawarada: *Diam. Relat. Matter.* **14** (2005) 1936.
- 5) H. Umezawa, T. Takenouchi, Y. Takano, K. Kobayashi, M. Nagao, I. Sakaguchi, M. Tachiki, T. Hatano, G. Zhong, and M. Tachiki: *cond-mat/0503303*.
- 6) H. Mukuda, T. Tsuchida, A. Harada, Y. Kitaoka, T. Takenouchi, Y. Takano, M. Nagao, I. Sakaguchi, and H. Kawarada: to be published in *Science and Technology of Advanced Materials* (Elsevier, 2006).
- 7) G. Baskaran: *cond-mat/0404286*, to appear in *J. Supercond.* (2006).
- 8) G. Baskaran: *cond-mat/0410296*.
- 9) E. Bustarret, J. Kačmarčík, C. Marcenat, E. Gheeraert, C. Cytermann, J. Marcus, and T. Klein: *Phys. Rev. Lett.* **93** (2004) 237005.
- 10) V. A. Sidorov, E. A. Ekimov, S. M. Stishov, E. D. Bauer, and J. D. Thompson: *Phys. Rev. B* **71** (2005) 060502(R).
- 11) K. Ishizaka, R. Eguchi, S. Tsuda, T. Yokoya, T. Kiss, T. Shimojima, T. Togashi, S. Watanabe, C.-T. Chen, C. Q. Zhang, Y. Takano, M. Nagao, I. Sakaguchi, T. Takenouchi, H. Kawarada, and S. Shin: *cond-mat/0604370*.
- 12) T. Yokoya, T. Nakamura, T. Matsushita, T. Muro, Y. Takano, M. Nagao, T. Takenouchi, H. Kawarada, and T. Oguchi: *Nature (London)* **438** (2005) 648.
- 13) H. Fukuyama: *J. Supercond. Novel Magn.*, to appear (2006).
- 14) A. K. Ramdas and S. Rodriguez: *Rep. Prog. Phys.* **44** (1981) 1297.
- 15) H. Kim, A. K. Ramdas, S. Rodriguez, M. Grimsditch, and T. R. Anthony: *Phys. Rev. Lett.* **83** (1999) 4140.
- 16) L. Boeri, J. Kortus, and O. K. Anderson: *Phys. Rev. Lett.* **93** (2004) 237002.
- 17) K. W. Lee and W. E. Pickett: *Phys. Rev. Lett.* **93** (2004) 237003; *Phys. Rev. B* **73** (2006) 075105.
- 18) X. Blase, C. Adessi, and D. Connétable: *Phys. Rev. Lett.* **93** (2004) 237004.
- 19) J. Nakamura, E. Kabasawa, N. Yamada, Y. Einaga, D. Saito, H. Issiki, S. Yugo, and R. C. C. Perera: *Phys. Rev. B* **70** (2004) 245111.
- 20) J. Nakamura, T. Oguchi, N. Yamada, K. Kuroki, K. Okada, Y. Takano, M. Nagao, I. Sakaguchi, H. Kawarada, R. C. C. Perera, and D. L. Ederer: *cond-mat/0410144*.
- 21) D. Wu, Y. C. Ma, Z. L. Wang, Q. Luo, C. Z. Gu, N. L. Wang, C. Y. Li, X. Y. Lu, and Z. S. Jin: *Phys. Rev. B* **73** (2006) 012501.
- 22) T. Oguchi: private communication.
- 23) H. J. Xiang, Z. Li, J. Yang, J. G. Hou, and Q. Zhu: *Phys. Rev. B* **70** (2004) 212504.
- 24) Y. Ohta, T. Shirakawa, S. Horiuchi, and H. Fukuyama: to appear in *Proceedings of M²S-HTSC, Dresden, 2006*.
- 25) B. Velicky, S. Kirkpatrick, and H. Ehrenreich: *Phys. Rev.* **175** (1968) 747.
- 26) F. Yonezawa: *Prog. Theor. Phys.* **40** (1968) 734.
- 27) R. J. Elliott, J. A. Krumhansl, and P. L. Leath: *Rev. Mod. Phys.* **46** (1974) 465.
- 28) H. Fukuyama: *Phys. Rev. B* **5** (1972) 2872.
- 29) H. Fukuyama: *Phys. Rev. B* **8** (1973) 4288.
- 30) P. W. Anderson: *J. Phys. Chem. Solids* **11** (1959) 26.
- 31) K. Ishizaka, R. Eguchi, S. Tsuda, T. Kiss, T. Shimojima, T. Yokoya, S. Shin, T. Togashi, S. Watanabe, C.-T. Chen, C. Q. Zhang, Y. Takano, M. Nagao, I. Sakaguchi, T. Takenouchi, and H. Kawarada: to be published in *Science and Technology of Advanced Materials* (Elsevier, 2006).
- 32) J. P. Carbotte: *Rev. Mod. Phys.* **62** (1990) 1027.
- 33) D. W. Taylor: *Phys. Rev.* **156** (1967) 1017.
- 34) R. Alben, M. Blume, H. Krakauer, and L. Schwartz: *Phys. Rev. B* **12** (1975) 4090.
- 35) R. Alben, M. Blume, and M. McKeown: *Phys. Rev. B* **16** (1977) 3829.
- 36) S. Maekawa and H. Fukuyama: *J. Phys. Soc. Jpn.* **51** (1981) 1380.
- 37) J. M. Graybeal and M. R. Beasley: *Phys. Rev. B* **29** (1984) 4167.
- 38) J. A. Sanjurjo, E. Lopez-Cruz, P. Vogl, and M. Cardona: *Phys. Rev. B* **28** (1983) 4579.
- 39) V. A. Gubanov, E. A. Pentaleri, C. Y. Fong, B. M. Klein: *Phys. Rev. B* **56** (1997) 13077.
- 40) P. Rodriguez-Hernandez, M. Gonzales-Diaz, A. Munoz: *Phys. Rev. B* **51** (1995) 14705.
- 41) K. Karch, P. Pavone, W. Windl, O. Schutt, and D. Strauch: *Phys. Rev. B* **50** (1994) 17054.
- 42) A. A. Lebedev: *Semiconductors* **33** (1999) 107.
- 43) H. Kuwabara and S. Yamada: *Phys. Stat. Solidi A* **30** (1975) 739.
- 44) C. Persson and U. Lindefelt: *J. Appl. Phys.* **82** (1997) 5496.